



Grid Cells and the Entorhinal Map of Space

Nobel Lecture, 7 December 2014

by Edvard I. Moser

Centre for Neural Computation and Kavli Institute for Systems Neuroscience;
Norwegian University of Science and Technology, Norway.

1. FROM PSYCHOLOGY TO NEUROPHYSIOLOGY—AND BACK

In 1983, May-Britt and I signed up for psychology studies at the University of Oslo. We wanted to understand the neural basis of behaviour. We were intrigued by the great learning theories from the 1930s, 1940s and 1950s and studied the work of J.B. Watson, C.L. Hull, B.F. Skinner and E.C. Tolman (Fig. 1). We found it fascinating that psychology had reached a level where application of the basic laws of the field made it possible to control long sequences of behaviour in animals.

Yet, while the scientific rigour of behaviourism attracted us, we were at the same time disappointed by the fact that physiology was deliberately left out from most behaviourist theories, due to lack of both methods and concepts. Karl Lashley's search for the neural basis of memory at the peak of the behaviourist era was a brave exception and defined the beginning of the merge between psychology and physiology (Lashley, 1929, 1950). However, it was only with Donald O. Hebb, from the end of the 1940s, that behaviour was linked conceptually to neurophysiology (Hebb, 1949). Hebb's ideas on cell assemblies and plasticity inspired an entire new generation of physiologists and psychologists with an interest in learning and memory. The new interest in learning culminated decades later by the discovery of key synaptic mechanisms of memory, as recognised by the 2000 Nobel prize to Eric Kandel (Kandel, 2000).

The potentials of this development—from the laws of learning to its detailed synaptic implementation—really caught May-Britt and me. The wish to bring



FIGURE 1. All three 2014 Nobel Prize winners in Physiology or Medicine stand on the shoulders of E.C. Tolman. Based on experiments on rats running in various types of mazes, Tolman suggested from the 1930s to the 1950s that animals form internal maps of the external environment. He referred to such maps as cognitive maps and considered them as mental knowledge structures in which information was stored according to its position in the environment (Tolman, 1948). In this sense, Tolman was not only one of the first cognitive psychologists but he also directly set the stage for studies of how space is represented in the brain. Tolman himself avoided any reference to neural structures and neural activity in his theories, which was understandable at a time when neither concepts nor methods had been developed for investigations at the brain-behaviour interface. However, at the end of his life he expressed strong hopes for a neuroscience of behaviour. In 1958, after the death of Lashley, he wrote the following in a letter to Donald O. Hebb when Hebb asked him about his view of physiological explanations of behaviour in the early days of behaviourism: "I certainly was an anti-physiologist at that time and am glad to be considered as one then. Today, however, I believe that this ('physiologising') is where the great new break-throughs are coming." Photo: courtesy of the Department of Psychology, UC Berkeley. Letter: Steve Glickman, UC Berkeley.

physiology to psychology was a wish that we shared with many of our forerunners (Fig. 1), and it was the beginning of a long journey for the two of us, a journey that was aided tremendously, at different stages, by many mentors and collaborators, particularly our Ph.D. supervisor Per Andersen.

Somewhat independently of Hebb's approach to physiology, the psychology-physiology boundary was broken from the other side—by two pioneers of physiology—David Hubel and Torsten Wiesel (Fig. 2)—who in the late 1950s bravely started to record activity from single neurons in the cortex, the origin of most of our intellectual activity. Inserting electrodes into the primary visual cortex of awake animals, they discovered how activity of individual neurons could be related to specific elements of the visual image (Hubel and Wiesel, 1959, 1962, 1977). This work set the stage for decades of investigation of the neural basis for vision and helped the emergence of a new field of cortical computation. Their insights at the low levels of the visual cortex provided a window into how the cortex might work. As a result of Hubel and Wiesel's work, parts of the coding mechanism for vision are now understood, almost 60 years after they started their investigations.



FIGURE 2. David H. Hubel and Torsten N. Wiesel broke the physiology-psychology boundary from the physiology side. By identifying the elementary neural components of the visual image at low levels of the visual cortex, they showed that psychological concepts, such as sensation and perception, could be understood through elementary interactions between cells with specific functions. Courtesy of Torsten N. Wiesel.

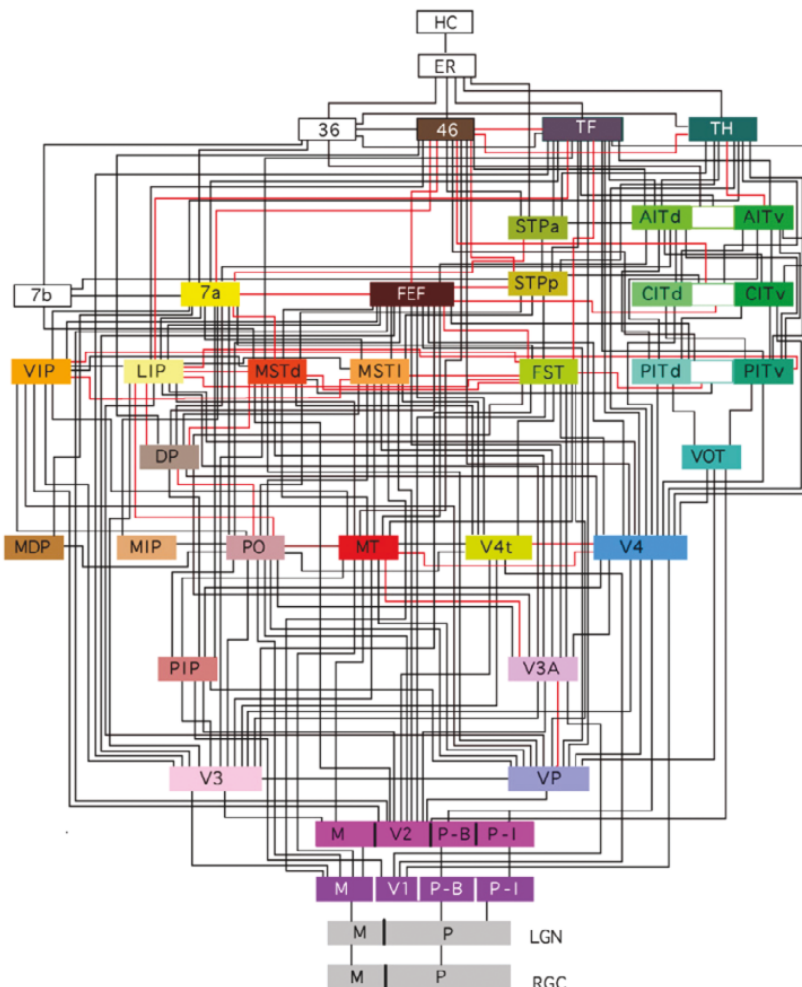


FIGURE 3. Hierarchical map of visual regions of the cortex showing visual input at the bottom (RGC, retinal ganglion cells; LGN, lateral geniculate nucleus) and entorhinal cortex (ER) and hippocampus (HC) at the top. Hubel and Wiesel's work led to revolutionary insights at the low levels of the hierarchy. As we move upwards in the hierarchy, correlations between neural activity and events or patterns in the outside world disappear rapidly. The cells of the hippocampal-entorhinal space system, at the peak of the hierarchy, represent a rare exception. Reproduced, with permission, from Felleman and van Essen (1991).

However, most of our knowledge of the cortex is confined to the entry level, at the early stages of sensory systems. As we move upwards in the cortical hierarchy (Fig. 3), clear correlates to the external world become rare and scientists often get lost or they avoid these areas. There are a few exceptions though. At

higher levels of the visual system, there are cells that respond to sophisticated combinations of elementary features, as well as ethologically important objects such as hands and faces (Gross et al., 1969, 1972; Bruce et al., 1981; Perrett et al., 1982; Tanaka et al., 1991; Tsao et al., 2005). The most striking example, perhaps, appears at the very peak of the sensory hierarchy, in the hippocampus, as deep into the cortex as you can get. In 1971, John O'Keefe and John Dostrovsky discovered that hippocampal cells tend to fire specifically when animals are at certain locations of the environment (O'Keefe and Dostrovsky, 1971; O'Keefe, 1976; Fig. 4). In small environments, each cell usually has a single firing location. Collectively a bunch of co-localised cells cover all areas of the environment, giving rise to the idea that place cells are part of an internal Tolmanian map of space (O'Keefe and Nadel, 1978). The strong relationship between neural activity and a property of the outside world—the animal's location—suggested that it was indeed possible to link physiology and psychology even in brain systems far away from sensory inputs and motor outputs.

The potential for understanding a higher brain function brought May-Britt and me to John O'Keefe's lab in 1996. During a period of three months, John generously taught us everything about place cells and how they were studied and we then went back to Norway, to Trondheim, to set up our own new lab. One of our hopes was to find out how the place signal was generated.

In this overview, I will first review the events that led up to the discovery of grid cells and the organisation of a grid cell-based map of space in the medial

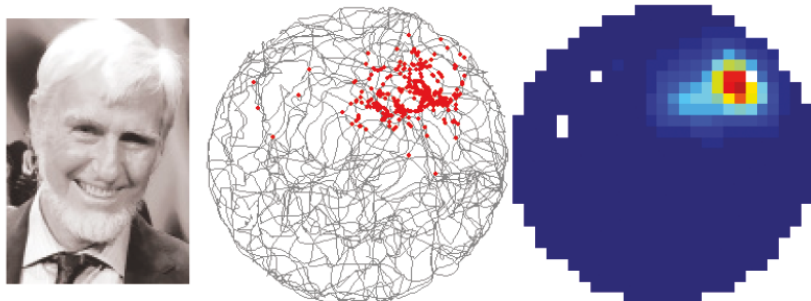


FIGURE 4. John O'Keefe (left) discovered place cells in the hippocampus (O'Keefe and Dostrovsky, 1971). Place cells (middle and right) are cells that fire specifically when an animal is at a certain location in its local environment. In the middle diagram, the animal's path in a circular recording enclosure is shown in grey; firing locations of individual spikes are shown for a single place cell in red. To the right, the firing rate of the same cell is color-coded (blue, low rate; red, high rate). In larger environments, place cells usually have more than one firing field (Fenton et al., 2008).

entorhinal cortex. Then, in the second part, I will present recent work on the interactions between grid cells and the geometry of the external environment, the topography of the grid-cell map, and the mechanisms underlying the hexagonal symmetry of the grid cells.

2. MOVING INTO UNKNOWN TERRITORY—THE ENTORHINAL CORTEX

The hippocampal circuit consists of several stages—including dentate gyrus, CA3 and CA1—which are connected more or less in a unidirectional sequence parallel to the transverse axis of the hippocampus (Andersen et al., 1971; Fig. 5). Each stage in this circuit receives additional direct input from the entorhinal cortex. In the 1990s, neural recordings from the entorhinal cortex suggested that cells in this area have broad and dispersed firing fields, quite different from the sharp and confined fields of the CA1 area of the hippocampus (Barnes et al., 1990; Quirk et al., 1992; Frank et al., 2000). A common idea until the end of the 1990s was therefore that the place signal was computed, or at least sharpened, between the entorhinal cortex and CA1, within the intrinsic circuit of the hippocampus, at the level of dentate gyrus and CA3.

To determine if place fields were formed in the intrahippocampal circuit, we worked together with neuroanatomist Menno Witter, then at the Free University of Amsterdam. Our first project was to isolate the CA1 from the earlier stages of the hippocampus, using chemical inactivation (Brun et al., 2002; Fig. 5). Following isolation of CA1 from the earlier stages, we could demonstrate that only direct inputs from the entorhinal cortex were left. We then recorded place cells in CA1 of this preparation. In spite of the rather complete removal of intrinsic excitatory input, cells with place fields could still be identified in CA1, although the firing fields were often somewhat more blurred than in control animals (Fig. 6). The findings suggested that spatial information was computed either by the CA1 circuit alone, which we thought was unlikely due to its predominant feed-forward architecture, or that the signal came in to the CA1 via direct inputs from the entorhinal cortex that bypassed the CA3. It made sense to record activity in the entorhinal cortex to settle this issue.

In collaboration with Menno Witter and our two students Marianne Fyhn and Sturla Molden, we then implanted electrodes in the dorsocaudal part of medial entorhinal cortex, far dorsal to the region where entorhinal activity had been recorded in earlier studies. We chose this region of the entorhinal cortex because it projects to the dorsal hippocampus, which is where most of the place-cell activity had been recorded at that time (Witter et al., 1989; Dolorfo and Amaral, 1998). Cells in this area of the entorhinal cortex had clearly defined

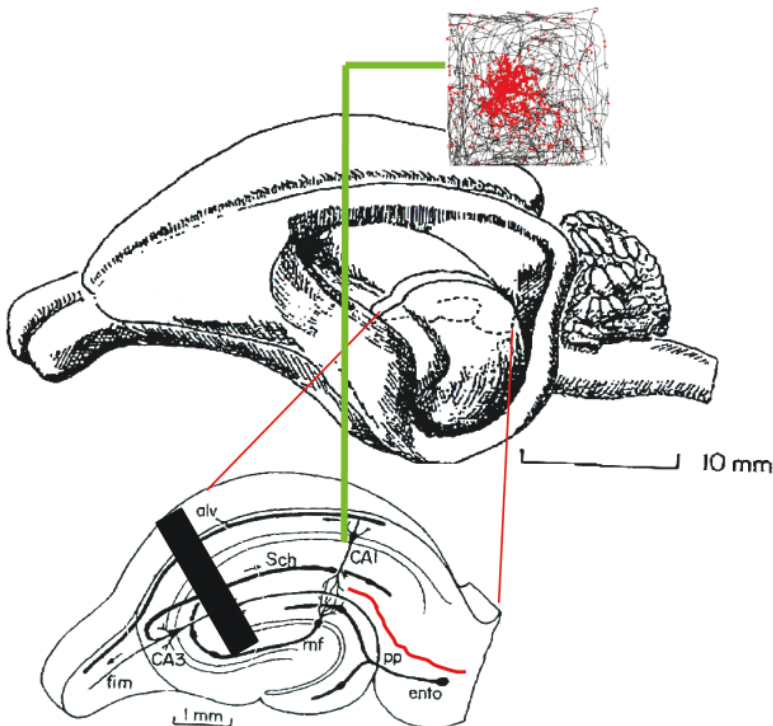


FIGURE 5. Location of recording electrode and lesion in the experiment that led us to move out of the hippocampus, to the entorhinal cortex (Brun et al., 2002). The upper image shows the hippocampus as a cashew nut-shaped structure underneath the cortical surface in a rodent brain. The lower image shows a transverse transection through the hippocampus. The major subfields of the hippocampal region, including entorhinal cortex (ento), CA3 and CA1, are indicated. Connections through the hippocampus are largely unidirectional, from entorhinal cortex through dentate gyrus and CA3 to CA1 (the intrinsic circuit) or directly from entorhinal cortex to each individual subfield, as indicated in red for the connection to CA1. The position of a tetrode in the CA1 area is indicated, as is the place field for a cell in this area (spike locations shown as red dots on black trajectory, as in Fig. 4). The black bar indicates the location of lesions that interrupted the intrinsic circuit and disconnected CA1 from the CA3 in the Brun study. The hippocampus diagram is modified from Andersen et al. (1971).

firing fields (Fyhn et al., 2004). Many cells had firing patterns that were as sharp as those of place cells in the CA1 of the hippocampus but they were different (Fig. 7). First of all each cell had many firing fields. Second the fields were not at random positions in the environment but neighbouring fields rather seemed to be separated by a constant distance. There was a peculiar regularity about this pattern but we did not understand the underlying algorithm.

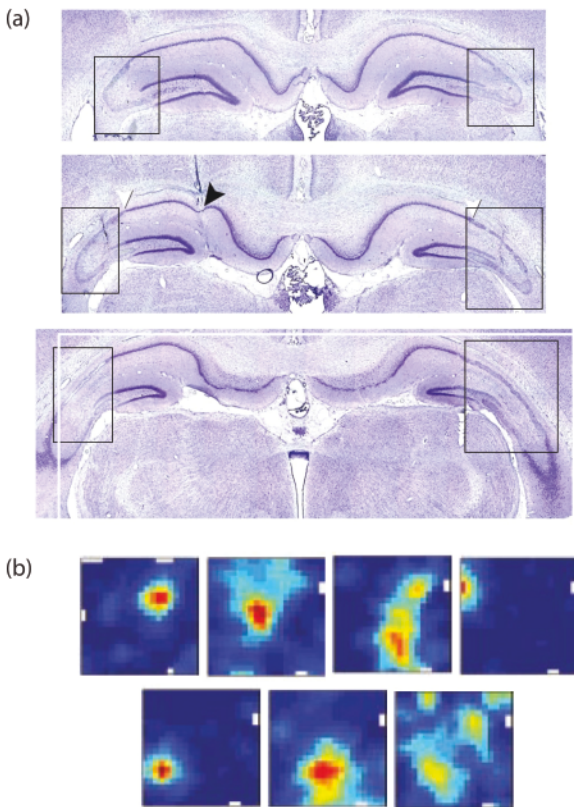


FIGURE 6. Place cells in CA1 after interruption of the intrinsic hippocampal circuit. (a) Nissl-stained coronal brain sections showing location of lesion and tetrodes in a single animal. CA3 of the dorsal hippocampus was almost entirely removed (outline of lesion indicated by rectangular boxes). Arrowhead indicates location of tips of the tetrodes in the CA1 pyramidal cell layer. (b) Colour-coded firing rate maps showing place fields of 7 representative CA1 pyramidal cells in a square enclosure (red, peak rate; dark blue, no firing; colour code as in Fig. 4). Same animal as in (a). Reproduced, with permission, from Brun et al. (2002).

3. GRID CELLS AND THEIR FUNCTIONAL ORGANISATION

In 2005, with our students Torkel Hafting, Marianne Fyhn and Sturla Molden, we were able to describe the structure of the firing pattern. Using larger environments than in the past, we could clearly see that the firing pattern was periodic (Hafting et al., 2005). The multiple firing fields of the cell formed a hexagonal grid that tiled the entire surface space available to the animal, much like the holes in a bee hive or a Chinese checkerboard (Fig. 8). Many entorhinal cells

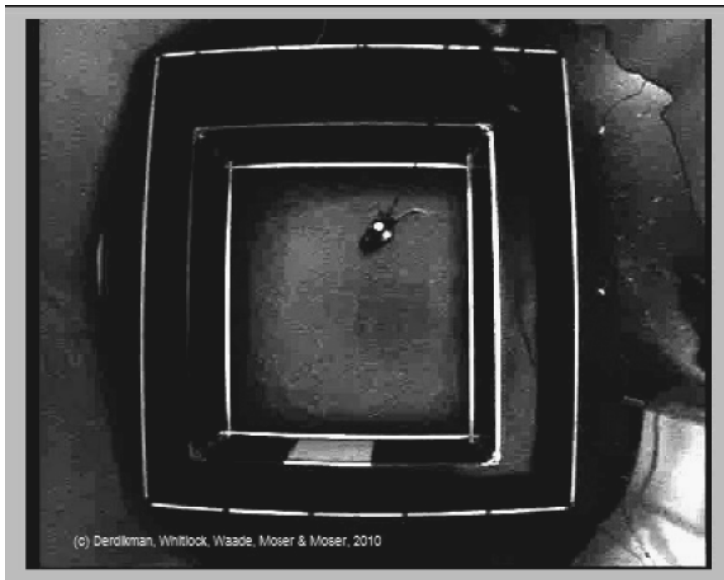


FIGURE 7. Movie showing firing location of a single cell in the medial entorhinal cortex while the rat is chasing chocolate sprinkles in a square recording enclosure. Individual spikes are displayed as white dots at the location of firing. Note the appearance of multiple firing fields and the apparently fixed distance between neighbouring fields. See nobelprize.org for the movie.

fired like this, and we named them grid cells. We were excited about the grid-like firing pattern, both because nothing like it exists in the sensory inputs to the animal, suggesting that the pattern is generated intrinsically in the entorhinal cortex or neighbouring structures, and because such a regular pattern provides a metric to the brain's spatial map—a metric that had been missing in the place map of the hippocampus (O'Keefe, 1976).

Grid cells were abundant in all cell layers of the medial entorhinal cortex (Sargolini et al., 2006). The most regular cells were in layer II, where approximately half of the cell population passed the criteria for grid cells. But grid cells came in different varieties (Fig. 9). There were at least three parameters of variation (Hafting et al., 2005). First, the cells differed in phase, or the x - y locations of the grid vertices. All possible grid phases were represented. Second, grid cells differed in scale, or spatial frequency, or the size of the fields and the spacing between them. In the grid cells with the smallest scale, the distance between the firing fields was only 30 cm. Other cells had field distances of more than a meter. Finally, grid cells sometimes had different orientations, i.e., the axes of the grid

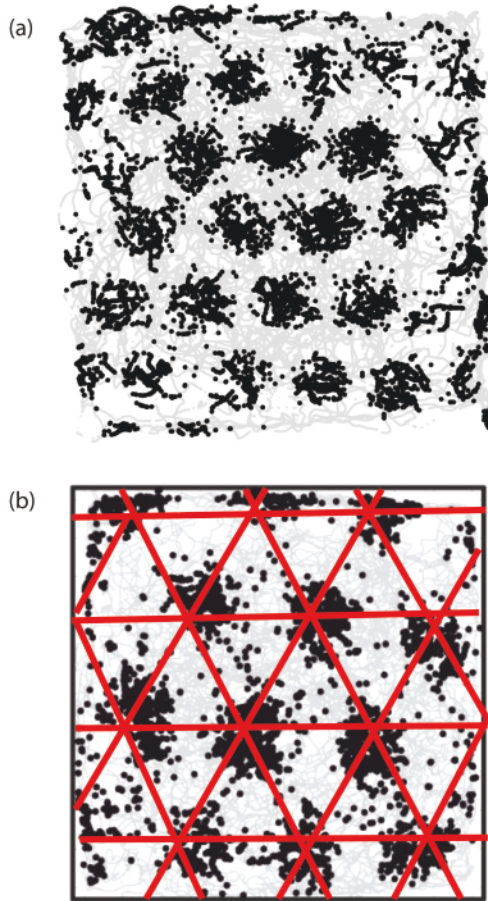


FIGURE 8. Firing pattern of grid cells. (a) Spatially periodic firing pattern of an entorhinal grid cell during 30 min of foraging in a 220 cm wide square enclosure. The trajectory of the rat is shown in grey, individual spike locations in black. (b) Firing pattern of a grid cell in a 1 m wide enclosure. Symbols as in (a) but with red lines superimposed to indicate the hexagonal structure of the grid. Modified from Stensola et al. (2012) and Hafting et al. (2005), respectively.

were tilted at different degrees from a reference axis such as a wall of the recording environment.

Following the discovery of the new cell type, we set out to determine how the grid map was organised according to parameters such as phase and scale (Hafting et al., 2005). Let me begin with the phase of the grid cells, i.e. the locations of the grid vertices. Do neighbouring cells have the same phase, or are their phase relationships random? Cells that were recorded on the same tetrode generally had different grid phases (Fig. 10). The firing locations of cells from

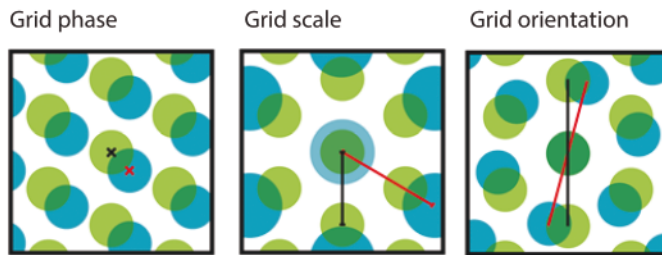


FIGURE 9. There are at least three parameters of variation among grid cells: grid phase, grid scale and grid orientation. Differences in phase, scale and orientation are illustrated for a pair of grid cells—one in green and one in blue. Grid phase refers to the x - y locations of the firing fields, grid scale is reflected in size of the firing fields and the distance between them (grid spacing), and grid orientation is determined by the angle of the grid axes relative to an external reference line (e.g. a wall of the recording box).

the same tetrode were apparently no more similar than those of cells that had been recorded on widely dispersed tetrodes. The findings suggested that, within the spatial resolution of the tetrode technique, grid phase is represented non-topographically. All grid phases appeared to be present within a small patch of the entorhinal network. The scattered representation is reminiscent of the

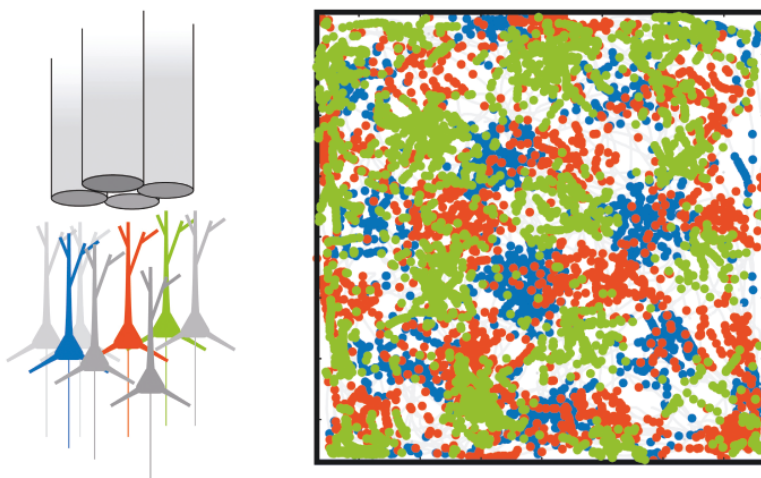


FIGURE 10. Grid phase appears to be organised non-topographically, at least within the resolution of the tetrode technique. Left, tetrode with cells that give rise to signals on the tetrode. Three grid cells are indicated with different colours. Right, firing fields of three grid cells recorded at the same tetrode location. There is apparently no correspondence between the grid phases of the three cells. The exact location of the three cells within the recording field of the tetrode cannot be determined from the tetrode signals. Modified from Hafting et al. (2005).

salt-and-pepper organisation of orientation-selective cells in rodents (Ohki et al., 2005; van Hooser et al., 2005), and of a number of other neural cortical representations such as odour maps in the piriform cortex (Stettler and Axel, 2009) or the place-cell map of the hippocampus (O'Keefe, 1976; Wilson and McNaughton, 1993).

In contrast to grid phase, the scale of the grid was mapped topographically at the macroscopic level. On average, grid spacing increased from dorsal to ventral medial entorhinal cortex. As the electrodes were moved downwards, we saw a progressive increase in the mean scale of the grid, reflected in the size of the fields as well as their separation (Fig. 11). The earliest data were not able to tell us whether this increase was smooth and gradual, or whether the grid increased in discrete steps. Because of limited cell sampling, we had to average the data across animals (Fyhn et al., 2004; Hafting et al., 2005), and it remained possible that averaging wiped out step-like increases that were present in individual animals.

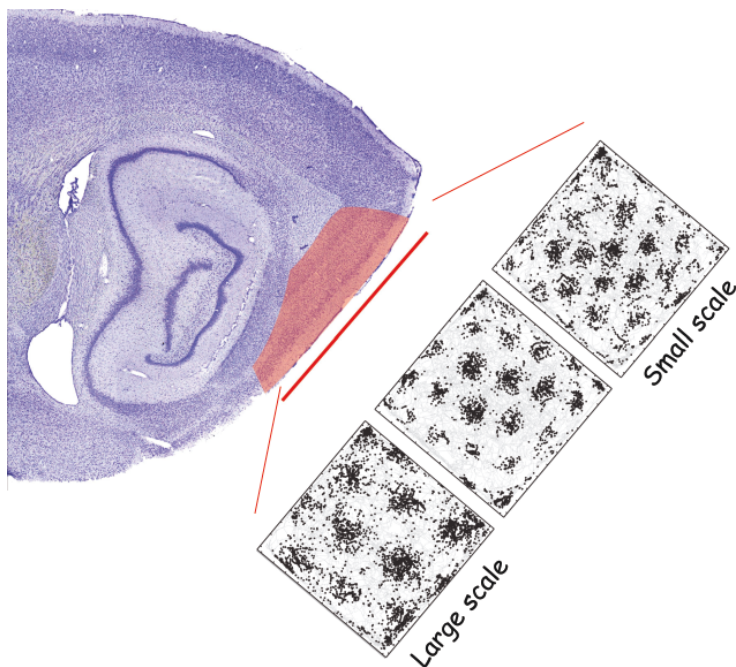


FIGURE 11. Topographical organisation of grid scale. The figure shows a sagittal brain section with medial entorhinal cortex indicated in red. Firing maps are shown for three grid cells recorded at successive dorso-ventral levels in medial entorhinal cortex. Note change from small scale to large scale along the dorso-ventral axis. Modified from Stensola et al. (2012).

In 2012, with Hanne and Tor Stensola and several other students, we were eventually able to determine the nature of the scale change (Stensola et al., 2012). We were now able to record up to almost 200 grid cells from the same animal, enough to determine if grid scale increases continuously or in a step-like manner. The recordings showed indeed that grid spacing increases in discrete steps (Fig. 12a). On average, grid spacing increased from dorsal to ventral, as we had observed before, but there were only four or five levels of spacing. We referred to each level as a module. As the electrodes were moved from dorsal to ventral, new modules were recruited in an additive manner, such that the most dorsal levels of medial entorhinal cortex had only the smallest module (M1), whereas more ventral levels had both M1 and M2, and even more ventral levels M1, M2 and M3. The number of cells in each module decreased substantially from M1 to M4 and M5. Thus, grid scale is organised topographically but the map consists of anatomically overlapping modules. The organisation is quite different from the strict anatomical separation of functionally similar cells in some primary sensory cortices.

What is the relationship between the grid scales of successive modules? To determine this we measured the ratio between values for grid spacing of each successive pair of modules (Fig. 12b). Despite considerable variation in the scale ratios, the mean ratio was almost constant, between 1.40 and 1.43. For each pair of modules, the scale of the larger module could be obtained by multiplying the scale of the smaller module by a constant factor, just like in a geometric progression. This way of organising grid scale might, according to theoretical analyses, be the optimal way to represent space at maximal resolution with a minimum number of cells (Mathis et al., 2012; Wei et al., 2013).

4. A UNIVERSAL MAP

As I approach the end of the historical part of my lecture, I want to draw your attention to the functional rigidity of the grid modules. In 2007, with our close collaborator Alessandro Treves from SISSA in Trieste and our students Marianne Fyhn and Torkel Hafting, we found that simultaneously recorded grid cells maintained scale, phase and orientation relationships across environments and experiences (Fyhn et al., 2007; Fig. 13a). We assessed the similarity of grid maps in square and circular environments, in the same room or in different rooms, by cross-correlating the rate maps of all recorded grid cells (Fig. 13b). Cross-correlation maps of cells from different environments had vertices that were spaced in a hexagonal grid pattern reminiscent of the grid pattern in individual cells (Fig. 13c). The maintenance of grid structure in the cross-correlation maps,

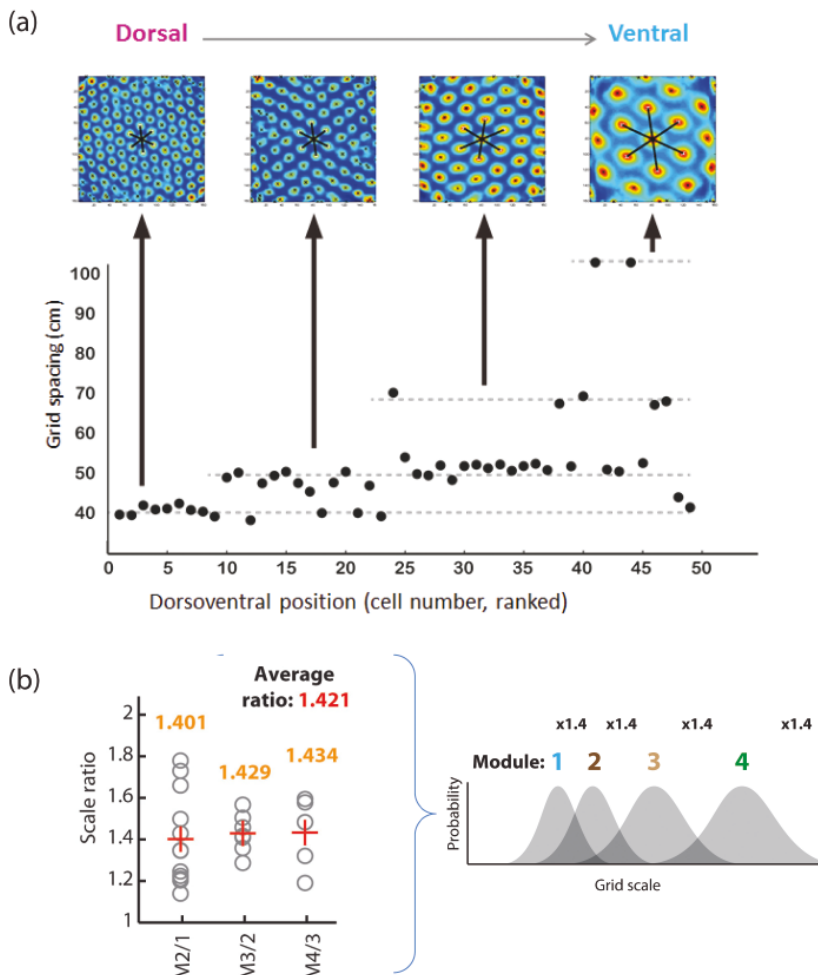


FIGURE 12. The grid map is modular. (a) Grid scale increases in discrete steps. Top, autocorrelograms for four cells belonging to different modules. Bottom, grid spacing for all grid cells of a single animal as a function of recording position along the dorso-ventral axis of medial entorhinal cortex. Each dot corresponds to one cell. Cells are rank-ordered from dorsal to ventral. Stippled lines indicate mean values for four discrete modules (modules M1-M4). Cells were assigned to modules through a k-means clustering algorithm. Arrows indicate module identity for the four example cells at the top. (b) Left, scale ratio of successive module pairs. Circles correspond to individual module pairs (32 modules, 11 rats). Mean scale ratios for module pairs are indicated in orange, grand mean in red. Right, schematic illustration of increase in grid scale across 4 modules. For each module, the mean scale value can be obtained by multiplying the scale of the preceding module by a fixed factor (1.4), as if module scales formed a geometric progression. Modified from Stensola et al. (2012) and Moser et al. (2014).

despite shifts in the absolute positions of the vertices, implies that cells keep spatial relationships across environments. If two cells have overlapping grid vertices in one environment, they will have overlapping vertices in another environment too; if their phases are opposite in one environment, they will be opposite in the other too. In 2012, after the discovery of modules, we observed that this rigidity always applied to cells within the same module, whereas cells from different modules might have unpredictable spatial relationships (Stensola et al., 2012). These findings suggested that a grid module operates like a universal map that does not care about the detailed content of the environment, much unlike maps of place cells, which change to completely different configurations whenever the animal moves to a different environment (Muller and Kubie, 1987). Simultaneous recordings from the hippocampus verified this difference. Cross-correlograms for hippocampal cells showed no reliable peaks (Fig. 13d), suggesting that the structure of simultaneously active place cells was highly different in the two environments (Fyhn et al., 2007).

Taken together, these observations point to a key difference between grid cells and place cells. Grid modules are universal and rigid—as would be expected by a metric for space—whereas place cells take on a variety of patterns, as would be expected if they also participate in memory for events associated with the locations stored in the place-cell maps (Moser et al., 2008, 2014).

Finally, how universal are grid cells across species? I can reassure you that grid cells are not unique to rats (Fig. 14). Grid cells also exist in mice (Fyhn et al., 2008). In 2011, Nachum Ulanovsky's group found them in Egyptian fruit bats (Yartsev et al., 2011), on a different branch of the phylogenetic tree (Fig. 14), then Elisabeth Buffalo's group found them in macaque monkeys (Killian et al., 2012), and then Iszhad Fried and Mike Kahana's group found them in humans (Jacobs et al., 2013). Thus, grid cells, like the other spatial cell types, exist across many mammalian orders and probably originated early in mammalian evolution, or before.

5. GRID CELLS AND THE GEOMETRY OF THE ENVIRONMENT

During the remainder of this lecture, I wish to share with you what trajectories our lab is following at the moment. I will briefly touch on three sets of new questions and data, much of which is still unpublished.

First I would like to ask how the grid pattern interacts with the environment. Grid cells are generated by intrinsic computations but to be useful for spatial mapping and navigation, they need to maintain a consistent relationship to the

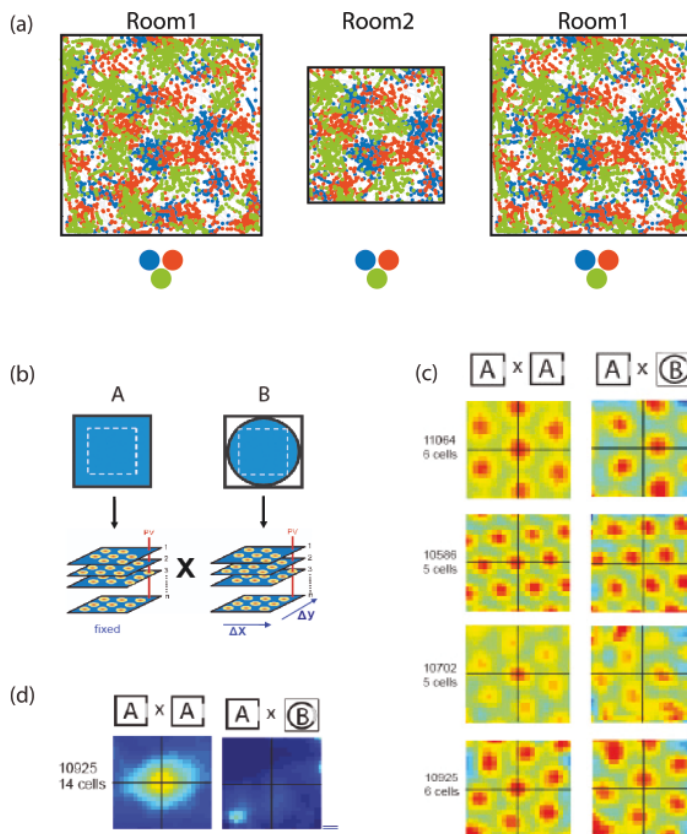


FIGURE 13. Universality of the grid map. (a) Schematic illustrating preservation of scale, phase and orientation relationships among grid cells when animals are tested in different environments. Firing patterns of three grid cells, each with a different colour, are copied across environments to illustrate that pattern relationships are maintained across rooms. (b) Illustration of cross-correlation method. For each environment A and B, rate maps for different cells were stacked into a three-dimensional matrix with space defined by x and y and cell identity by z . For each stack a population vector was defined for every single bin of x - y space. Pairs of population vectors were then correlated across environments by shifting one of the stacks in small increments along the entire x and y axes. (c) Cross-correlation matrices for ensembles of simultaneously recorded grid cells in the medial entorhinal cortex. Left, repeated trials in the same environment ($A \times A$); right, trials in different environments ($A \times B$). The peak of the cross-correlogram remains at the origin on repeated trials in the same environment but shifts to a different location in comparisons of different environments, at the same time as the grid structure of the correlation map is retained. This indicates that phase, scale and orientation relationships are maintained across the two environments whereas absolute phase or orientation are different (vertices are shifted). (d) Cross-correlation matrices for cells that were recorded in CA3 of the hippocampus. Note lack of structure in the hippocampal cross-correlation matrix for different environments, suggesting that decorrelated maps are retrieved in the two environments. Modified from Fyhn et al. (2007).

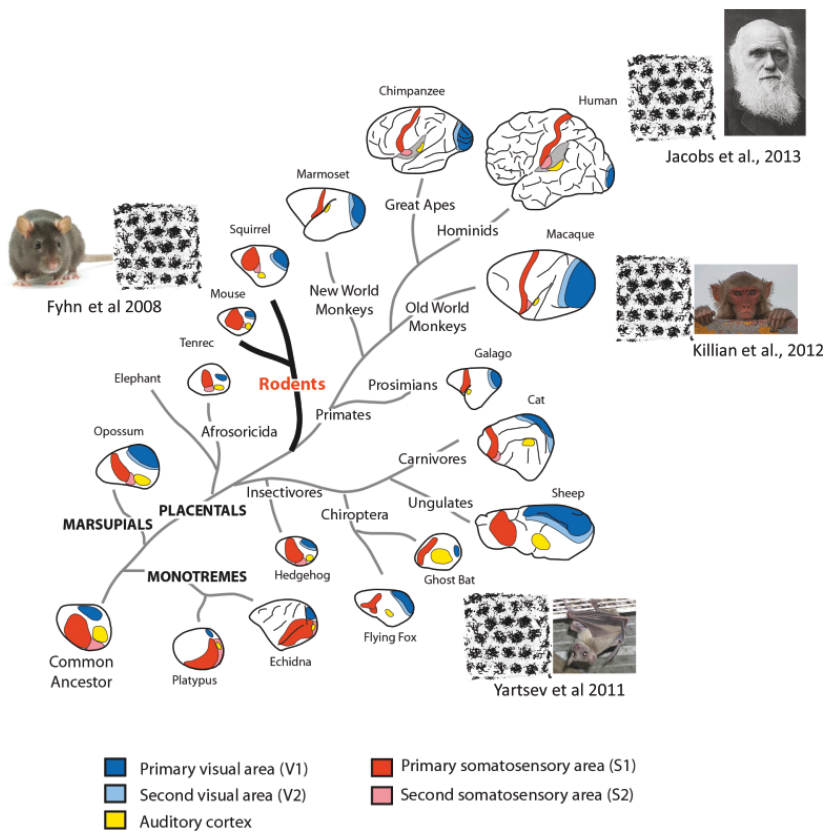


FIGURE 14. Grid-like cells have been reported in rodents, bats, monkeys and humans, suggesting they originated early in mammalian evolution. Adapted, with permission, from Krubitzer et al. (2011).

surroundings. They need to fire in the same locations each time the animal visits a particular place. They do so (Hafting et al., 2005) but how is this anchoring to the environment accomplished?

One clue to the mechanisms underlying the anchoring process is that the orientation of the grid pattern relative to the environment seems to be non-random (Stensola et al., 2012; Krupic et al., 2014). With our students Tor and Hanne Stensola we set out to explore this further (Stensola et al., 2015). Early on we were struck by the fact that the grid axes of different cells are more similar than expected by chance (Fig. 15a). In most cells the grid axes were slightly tilted with respect to the wall axes and the tilt seemed similar even between animals. In a sample of 587 grid cells from 6 different rats, tested in a 1.5 m wide square

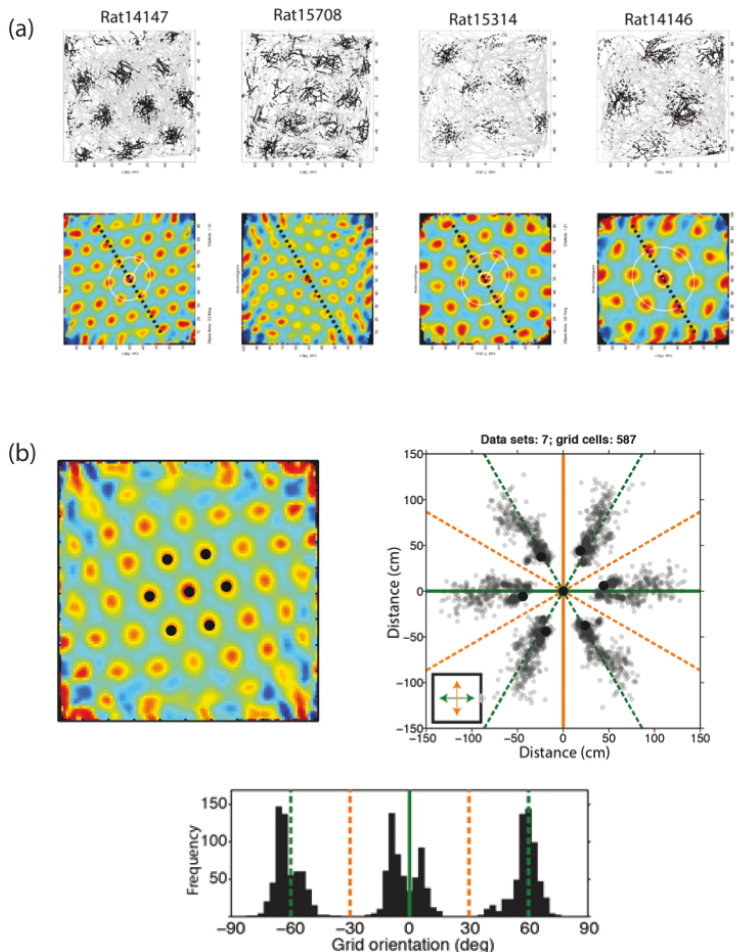


FIGURE 15. Alignment of grid patterns to external geometry. (a) Spike plots (top row) and spatial autocorrelograms (bottom row) for four representative grid cells recorded in different animals in the same 1.5 m wide square enclosure. Spike plots show trajectory in grey, with individual spike locations superimposed as black dots. Autocorrelogram is colour-coded, with correlation increasing from blue to red. Stippled line indicates orientation of one grid axis. Note similar orientation across cells and animals. (b) Top left: Spatial autocorrelogram of a single cell. Central peak and surrounding 6 peaks are indicated by black dots. Top right: Polar scatterplot showing distribution of grid orientation and grid spacing for 587 grid cells in the 1.5 m wide square enclosure. For each cell, the location of the 1+6 innermost fields in the spatial autocorrelogram (black dots in the left diagram) is shown (1+6 dots per cell; darkness indicates overlap). Distance from the centre is proportional to grid scale. Cardinal axes of the box are shown in orange and green. Stippled lines indicate 60-degree multiples of the cardinal axes. Bottom: Frequency distributions showing clustering of data in the polar scatterplot around each of the 3 axes defined by 60-degree multiples of the east-west orientation. Modified, with permission, from Stensola et al. (2015).

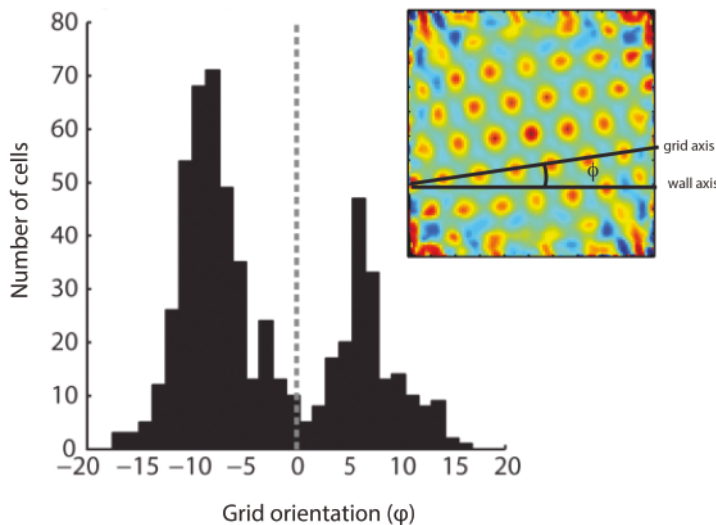


FIGURE 16. Frequency distribution showing orientation of the grid axis with the smallest offset from any of the box walls. This orientation is defined by the angle from the wall axis, as illustrated in the inset. Modified, with permission, from Stensola et al. (2015).

environment, only a limited range of grid orientations was represented. To illustrate the distribution, we made spatial autocorrelograms for each cell, identified for each autocorrelogram the centre and the surrounding 6 vertices, and then transferred, for each cell, these 7 points to a common circular scatterplot (Fig. 15b). The distribution was highly clustered, suggesting not only that grid cells had a small number of scale values, as would be expected from their scale modularity, but also that grid cells within a module had a similar orientation. Orientation was also shared across modules in many cases.

At first glance, it seemed as if grid cells line up with the symmetry axes of the environment, i.e. the north-south or east-west walls of the recording environment (Fig. 15b). Closer inspection suggested this was not the case, however (Fig. 16). On average, the grid axis nearest any of the wall axes had an offset of 5–10 degrees in either direction from the wall axis. In the 1.5 m box, grid orientations clustered around + or −7.5 degrees relative to the east-west wall. Almost no cells at all had offsets of 0 and 15 degrees. This invariant rotation of the grid pattern of course led us to ask if there is anything advantageous about 7.5 degree offsets and if 0 and 15 degrees were somehow disadvantageous.

The answers may be yes. 7.5 degrees is the offset that minimises symmetry between the grid pattern and the axes of the environment; it is *the* orientation

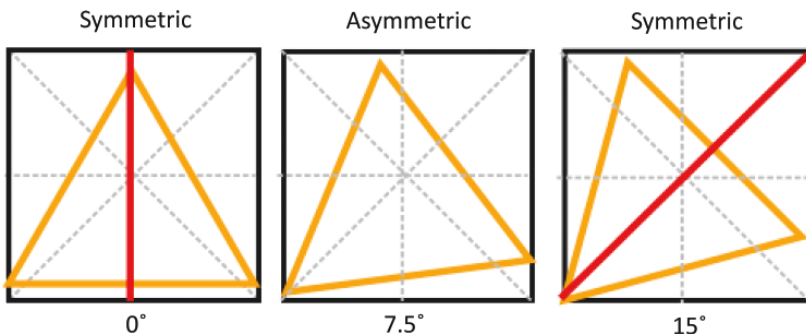


FIGURE 17. Overlap between symmetry axes of box and grid at 0° and 15° but not 7.5° . Stippled lines show symmetry axes of the box (2 cardinal axes and 2 diagonal axes). Orange lines indicate symmetry axes of the grid pattern at different degrees of offset. Red lines show symmetry axes common to box and grid. Note that symmetry axes of box and grid are maximally different when the grid is rotated 7.5° from one of the walls. 7.5° rotation may thus cause maximal disambiguation of grid patterns along orthogonal walls of the environment. Reproduced, with permission, from Stensola et al. (2015).

that causes maximal dissimilarity between patterns along the two wall axes (Fig. 17). In contrast, at 0 and 15 degrees, the box and the grid have common axes, and the grid pattern would look similar along some of the wall pairs. It might be then, that the offset is developed and maintained by the fact that it causes maximal disambiguation of activity patterns across similar regions of the environment.

What could generate such a consistent rotation of the grid pattern? One clue is that the rotation differs between the three grid axes. For the axis that is nearest one of the wall axes, the offset is on average 7.5 degrees, as I have shown. For the two other axes, however, the offset is smaller, with the axis furthest away from the wall axes showing only a 2 – 3 -degree rotation (Fig. 18ab). The differential rotation means that the grid must have lost its hexagonal symmetry and that the inner fields form an ellipse instead of a circle. A comparison of the ellipticity of the grid pattern and the rotational offset of the grid showed that the two effects were closely correlated, suggesting that they are caused by a single underlying mechanism (Fig. 18cd). So—what could this mechanism be?

We hypothesised that rotation and deformation of the grid could be due to shearing—a type of deformation where points on a plane are shifted along the shear axis in proportion to the distance from this axis (Mase, 1970). Shearing can be explained by starting out with an initially symmetric grid pattern, where the vertices of 6 neighbouring grid fields define a circle (Fig. 19, left). In the next

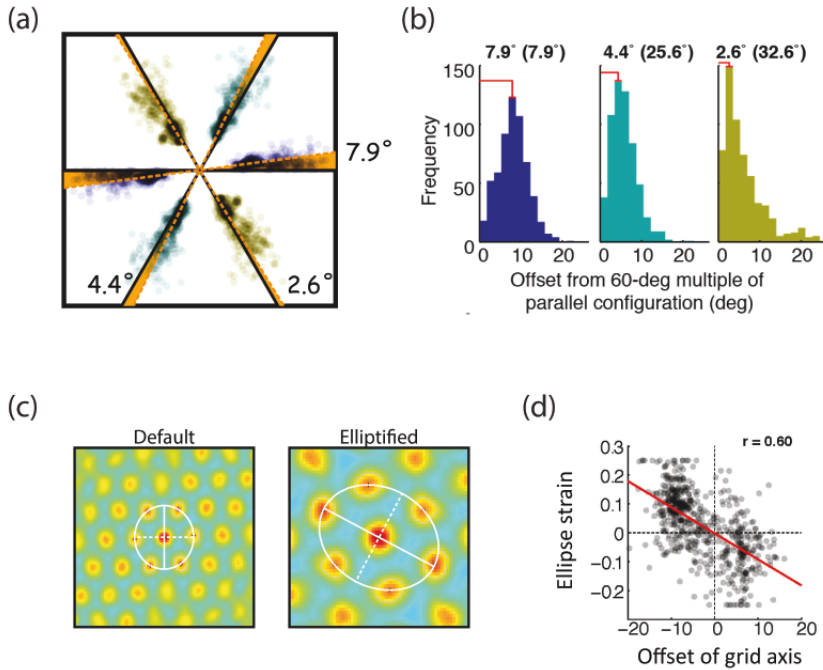


FIGURE 18. Rotational offset is accompanied by deformation. (a) Polar scatter plot (same data as in Fig. 16) showing axis-specific offset from the nearest wall axis or 60-degree multiples of it. Grids are reflected around the horizontal alignment axis for visualisation of differences between grid axes. Orange dashed lines show peak angular offset from 60° multiples (black lines) of parallel wall alignment (0°) for each axis. (b) Distribution of angular offset from nearest wall axis or 60-degree multiples of it. Peak angular offsets from nearest 60°-multiples are indicated at the top of each distribution (offset from respective nearest wall axis in brackets). (c) Spatial autocorrelogram showing symmetric and distorted grid pattern. Symmetry of the grid pattern is indicated by a white circle connecting the inner vertices of the autocorrelogram to the left. For the autocorrelogram to the right, which shows a deformed grid pattern, the vertex locations are defined instead by an ellipse. (d) Scatter plot showing strong correlation between angular offset of the grid and the strain of the ellipse fit shown in (c). Taken together, the covariation of grid rotation and grid deformation raises the possibility that they are reflections of a single mechanism. Modified, with permission, from Stensola et al. (2015).

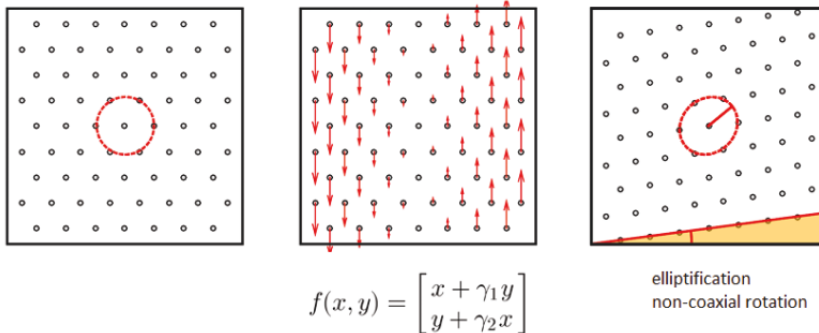


FIGURE 19. Rotation and deformation of the grid pattern may be caused by shearing, a type of deformation where points on a plane are shifted along a given axis in proportion to the distance from the axis. Shearing is illustrated here in three diagrams. The diagram to the left shows a grid pattern before any deformation. The inner vertices are identified by a red circle. The middle diagram shows the operation of shear forces. Red arrows indicate direction and strength of forces (length of arrow is proportional to strength). Shear forces are parallel to the east and west walls and operate in opposite directions on the two sides of the box. Transformation of the grid pattern due to simple shearing is given by the equation below. The result of the shear transform is shown to the right. Note strong rotation of the grid axis orthogonal to the shear forces (7.5° rotation, as illustrated by the red axis line) as well as deformation of the grid pattern (as indicated by transformation of the inner circle to an ellipse). Illustration by Tor Stensola.

step (Fig. 19, middle) we introduce shear forces, parallel to each of the east and west walls, and in opposite directions, with decreasing amplitude as we depart from the walls. Applying these forces converts the circle to an ellipse, at the same time as the axes of the grid pattern are rotated, with the strongest rotation occurring on the grid axis that is most offset from the shear axis (Fig. 19, right). The transformation of the pattern can be described as:

$$T(x, y) = \begin{bmatrix} 1 & \gamma_1 \\ \gamma_2 & 1 \end{bmatrix} \begin{bmatrix} x \\ y \end{bmatrix}$$

where γ_1 is the shear parameter along the y -axis, γ_2 the shear parameter along the x -axis, and x and y row vectors of initial coordinates of points in the plane. For simple shearing, only one of the shear parameters has a non-zero value. The strong relationship between elliptification and rotation in the simulations is reminiscent of the data. In fact, if simulated grids are elliptified exactly to the extent observed in the data, the accompanying rotation is 7.5 degrees, just as

in the data, strongly pointing to shearing as a mechanism for both the elliptic deformation and the rotational offset.

Thus, given that the effects could be reproduced by shearing on simulated grids, we turned to the real data and applied shear forces until we had minimised the ellipticity of the inner circle of the autocorrelogram, in the reverse direction of the forces that likely operated when the pattern was distorted in the first place (Fig. 20). As predicted, shearing completely removed the grid offset when the forces were applied with a direction that was orthogonal to the alignment axis,

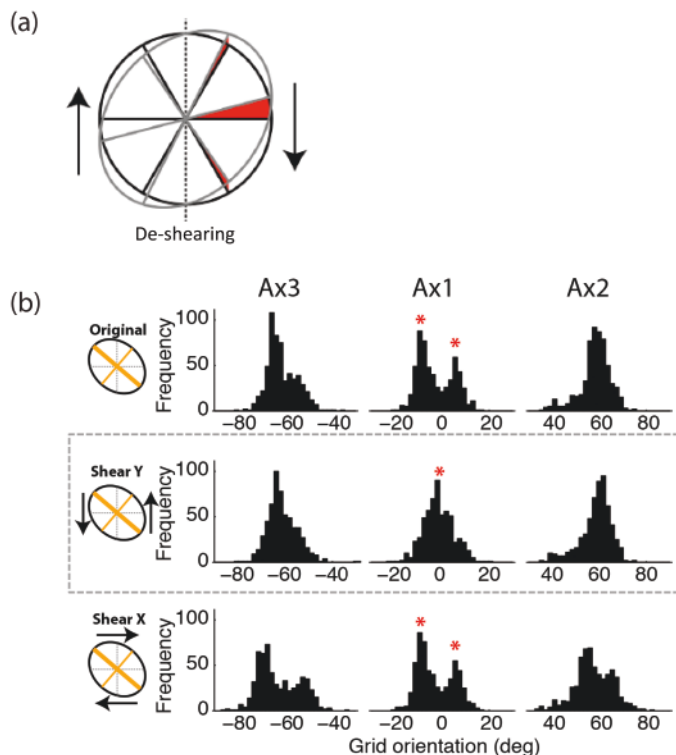


FIGURE 20. Effects of shearing are axis-specific. (a) Deformation and rotation of grid axes following shearing in the north-south direction. Shearing was applied in the reverse direction of the forces thought to operate as the grid was aligned in the first place. Shearing completely removed not only the deformation but also the offset of the grid axes. (b) Frequency distribution showing orientation for each grid axis before and after minimisation of ellipticity by simple shearing along the cardinal axes of the environment. Asterisks indicate peaks of the distribution for the axis nearest one of the cardinal axes. Note disappearance of orientation peaks at 7.5° following north-south shearing. Shearing in the orthogonal direction had minimal effects on the angular offset of the same grid axis. Modified, with permission, from Stensola et al. (2015).



FIGURE 21. Effects of shearing on rotation and deformation of a pattern can be illustrated with a stack of cards. Note grid axes on the side of the stack. Shear forces are imposed horizontally, with decreasing amplitude as distance from the top of the stack increases (top right; white arrows indicate strength of shear forces). The result of the shear transformation is shown at the bottom right. Note strong rotation of the grid axis orthogonal to the direction of the shear forces (black axis). The two other axes, with smaller offsets from the shear direction, show less rotation (red). Illustration by Tor Stensola.

i.e., with a north-south shear direction. Shearing in the east-west direction, parallel to the alignment axis, had no effect. The effect of shearing on rotation of the grid pattern can be illustrated in a stack of cards with grid axes displayed on the side of the stack (Fig. 21). When shear forces are applied along the top surface of the stack, with decreasing amplitude towards the centre, the grid is elliptified and the orthogonal axis is rotated more than the two other axes, which deviate less from the shear axis.

Taken together, these analyses clearly point to shearing as the mechanism for grid deformation and grid rotation. The findings imply that local boundaries exert distance-dependent effects on the grid pattern. Whether these forces are mediated through the existence of border cells, which intermingle with the grid cells (Savelli et al., 2008; Solstad et al., 2008), remains to be determined—but it is certainly a possibility (Hartley et al., 2000).

6. FINE-SCALE TOPOGRAPHY OF THE GRID-CELL NETWORK

In the next state-of-the-art part of my lecture, I wish to return to the anatomical organisation of the grid network. I showed you that within the resolution constraints of the tetrode technique, there seems to be no topography of grid phase, i.e. grid cells with different grid phases seem to be scrambled, at least at a macroscopic scale. However, tetrodes are thought to pick up spike signals within

a range of as much as 50–100 μm (Gray et al., 1995), corresponding to several cell widths. Thus we need other methods if we are to determine the topography of the grid-cell network at single-cell resolution.

One approach that *has* sufficient spatial resolution is two-photon fluorescent calcium imaging, which for some years has been applied to superficial cortical structures in anaesthetised animals (Stosiek et al., 2003; Kerr et al., 2005; Ohki et al., 2005, 2006) and awake head-fixed animals (Dombeck et al., 2007). With graduate student Albert Tsao we joined forces with Tobias Bonhoeffer at the Max Planck Institute for Neurobiology in Martinsried to image grid cells in head-fixed mice during navigation in a virtual environment where mice move forward in the environment in correspondence with their running movements on a stationary ball (Dombeck et al., 2007).

The first problem to solve was to get access to the medial entorhinal cortex. The medial entorhinal cortex lies at the worst possible place, at the back of the cortex, adjacent to the cerebellum, under the transverse sinus—apparently not readily accessible to surface imaging. The solution to the problem was to insert a prism between the cerebral cortex and the cerebellum, pushing back the cerebellum and leaving cortex, cerebellum, and sinus fully intact (Fig. 22; see also Heys et al., 2014, and Low et al., 2014). This allowed us to image the back surface of the cortex, i.e. the medial entorhinal cortex, from the top of the brain. Mice with prisms could then be injected in the medial entorhinal cortex with AAV virus encoding the fluorescent calcium indicator GCaMP6f, and three weeks later, when the indicator had expressed, the mice could be head-fixed and allowed to run in the virtual environment.



FIGURE 22. Calbindin-stained sagittal brain section showing that medial entorhinal cortex can be imaged from the local cortical surface by inserting a prism between the cerebral cortex and the cerebellum (red arrow). Stained by Flavio Donato.

With the prism approach the activity of individual cells in layer II of the medial entorhinal cortex could be viewed as the mouse ran through the virtual environment (Fig. 23a). Hundreds of cells could be imaged at the same time at cellular or subcellular resolution. A large fraction of the cells had spatial firing patterns in that they always lit up at constant positions on the track (Fig. 23b). Most cells had multiple firing fields. In some cases, the fields appeared at regular distances, suggesting that the cells were grid cells; however, in the majority of the space-modulated cells, the inter-field distances were variable (Fig. 23b, right). Could these non-periodic cells be grid cells? One problem is that the running track is one-dimensional whereas grid patterns are two-dimensional. Given what we now know about grid rotation, we cannot take for granted that grid cells line up with the direction of the track. If instead the activity on the track corresponds to a slice through a two-dimensional grid, in more than one direction, it might be difficult to tell if a cell is a grid cell or not, because in most slices the field distances would no longer be equal (Fig. 23b). Using an approach inspired by David Tank and colleagues (Domnisoru et al., 2013), we tried to solve this problem by determining the Euclidean distance between the firing pattern of a cell on the track and patterns in slices through all possible locations, orientations and deformations in a simulated two-dimensional grid pattern. Cells with low Euclidean distances between observed and simulated patterns were classified as grid cells.

Having a way to separate out grid cells, we then asked how they are organised in anatomical space. First we asked if grid cells were clustered. A circular window was moved across the entire available surface of the medial entorhinal cortex. For each step, we counted the number of grid cells inside the window. The number of grid cells counted per window was clearly higher than the number of grid cells in a shuffled image, where the identity of the cells in the image was scrambled randomly (Fig. 24), suggesting that the medial entorhinal cortex is organised as entangled small clusters of functionally similar cells. Whether grid cells within a cluster belong to the same grid module remains to be determined.

Finally, now that entorhinal two-photon imaging is operative, let me return to the question I started out with, which was whether neighbouring cells have a more similar grid phase than expected. So far the data suggest that the correlation between firing locations of neighbouring cells, spaced by 50–100 μm or less, is indeed higher than between randomly selected cell pairs. A recent report from another lab has shown the same (Heys et al., 2014). Thus, there is, in fact, some fine-scale topography in the grid map, but at a scale so small that tetrodes

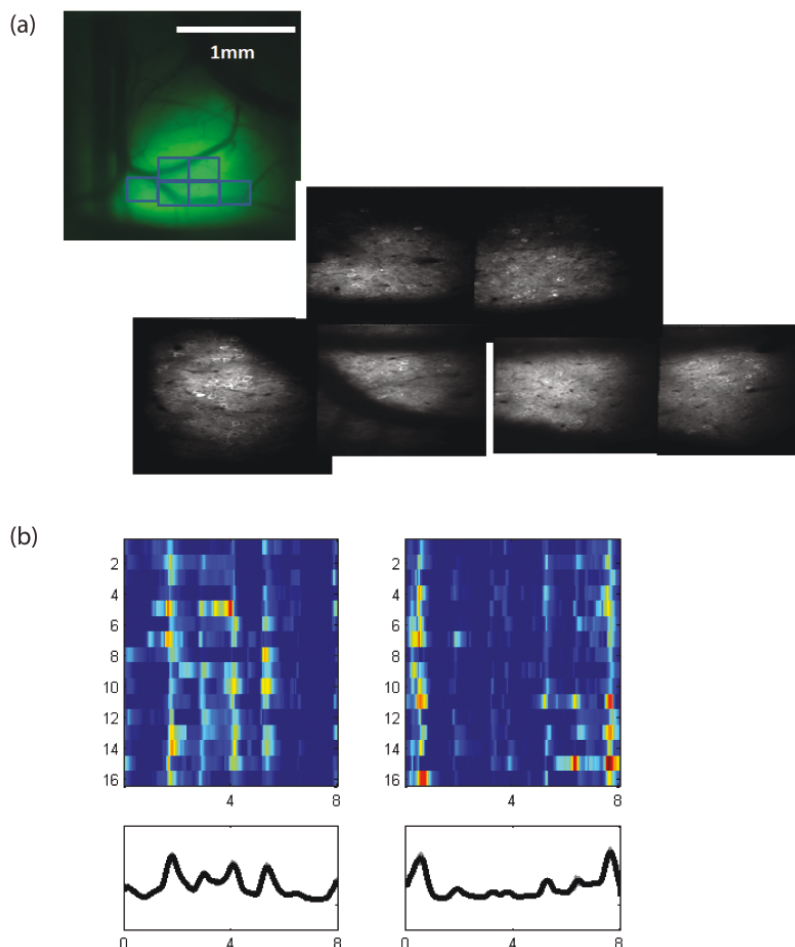


FIGURE 23. Two-photon imaging of medial entorhinal cortex cells during navigation in a virtual environment. (a) Top left: Surface view of medial entorhinal area seen through the prism. Note intact blood vessels. Bottom: magnified images showing instantaneous activity in each of the 6 rectangular windows of the top left image. White implies strong fluorescence. (b) Grid cells can be identified in the virtual linear environment as cells with periodic fields. Each colour-coded diagram shows activity as a function of distance along the track (0 to 8 m). Activity is colour-coded, with red indicating maximum activity and blue minimum. Each row shows one lap (all same cell). Left and right diagrams display opposite running directions for the same cell. Mean activity is shown in line diagrams below the colour plots. Note periodicity in the left diagram but not so much in the right diagram. Whether the sequence of activity fields corresponds to a slice through a two-dimensional grid was determined by comparing the activity on the virtual track with slices across all directions and locations of a simulated grid pattern. Euclidean distances between the observed pattern and the optimal slice through the simulated pattern were determined and cells were classified as grid cells if this distance was below a certain threshold. Illustrations made by Albert Tsao (Bonhoeffer-Moser collaboration).

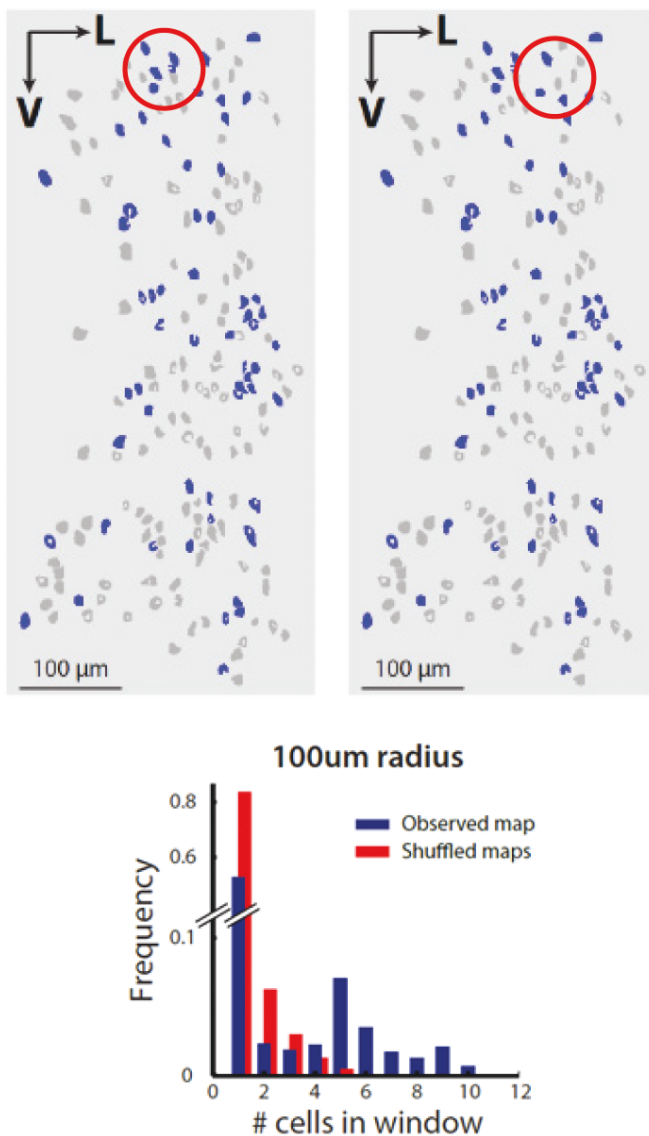


FIGURE 24. Grid cells are distributed but form functional clusters. Rectangles show an imaging window; blue cells are grid cells. Clustering of grid cells was determined by moving a circle in steps across the entire imaging window and counting, for each step, the number of grid cells in the window. Two example steps are shown (red circles). The number of grid cells was compared to the number obtained after random shuffling of cell identities (grid vs. non-grid) within the imaging window. The histogram shows the result of the counts. Note more frequent occurrence of large cell numbers in the real data than after shuffling, suggesting that grid cells are anatomically clustered. Illustrations made by Albert Tsao (Bonhoeffer-Moser collaboration).

do not detect it. The nature of this fine-scale topography, and its relation to cell identity, is still to be determined.

7. HOW IS THE GRID PATTERN GENERATED?

In the final part of my lecture, I would like to address one of the most important questions raised by the discovery of grid cells, which is how these hexagonal patterns are generated. There is a variety of computational models for the formation of grid patterns but most researchers now believe that attractor mechanisms are somehow involved. In a continuous attractor network, localized firing can be generated by mutual excitation between cells with similar firing locations (Fig. 25a; Tsodyks et al., 1995; McNaughton et al., 1996; Samsonovitch et al., 1997). Mutually connected cells may or may not be co-localised. When cells in the network are organised according to firing location, not anatomical location, excitatory connections between cells with similar firing fields maintain a localised bump of activity in the network, which is prevented from spreading in an uncontrolled manner by a surrounding ring of inhibition in a Mexican hat-like

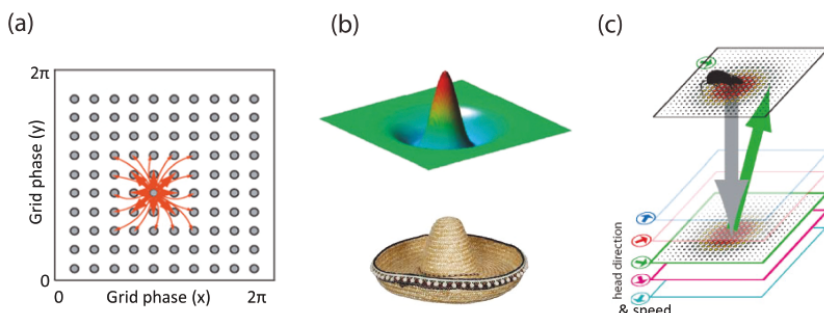


FIGURE 25. Mechanisms of spatially localised firing. Place-cell formation has been explained by continuous attractor dynamics (Tsodyks et al., 1995; McNaughton et al., 1996; Samsonovitch and McNaughton, 1997). In a continuous attractor network localized firing is generated by mutual excitation between cells with similar firing locations. In the network in (a), cells (circles) are arranged according to firing location in the square recording environment. Red arrows indicate excitatory connections. In addition, for each cell, there is an inhibitory surround that is wider than the radius of excitation. The inhibitory surround prevents uncontrolled spread of excitation and maintains a localised bump of activity. (b) The excitatory-inhibitory connectivity is often referred to as Mexican-hat connectivity. (c) Translation of the bump of activity across the network in accordance with movement in the external environment. Information about instantaneous displacement may reach grid cells via cells that monitor the animal's speed and direction in the environment. Modified, with permission, from McNaughton et al. (2006).

pattern (Fig. 25b). This bump of activity is then moved around in the neural network in accordance with the animal's movement in external space though inputs from cells that carry information about instantaneous speed (Fig. 25c). However, there is one problem with this model, which was originally developed for place cells. It explains localised activity but not the formation of hexagonal patterns.

During the years after the discovery of grid cells, several models were developed to explain how hexagonal firing could emerge in a continuous attractor network (Fuhs and Touretzky, 2006; McNaughton et al., 2006; Burak and Fiete, 2009). A common idea was that blobs of activity could emerge many places in the network, through mutual excitation and inhibitory surrounds, and that competitive interactions, i.e. inhibition, would keep these blobs away from each other. Mutual inhibition would then force the pattern into an equilibrium state where the blobs are as far away from each other as possible, which would be a hexagonal pattern (Fig. 26 and 27).

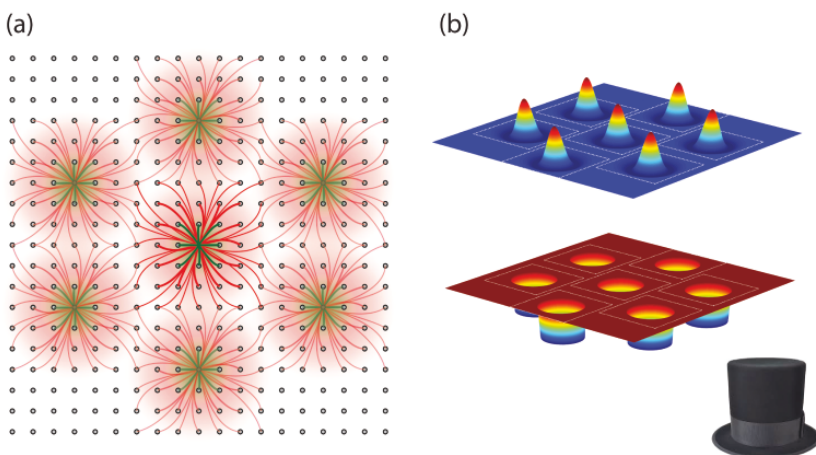


FIGURE 26. Continuous attractor models may explain origin of hexagonal structure in the grid pattern. (a) Competition between multiple self-exciting activity bumps on a neuronal lattice, each with an inhibitory surround. The competition may cause the network to self-organise into a hexagonal pattern, in which distances between bumps are maximised. Excitatory connections are green, inhibitory connections red. (b) Self-organisation into hexagonal patterns has been demonstrated not only for Mexican hat connectivity but also for networks consisting of cells that have all-or-none inhibitory connections with each other, without additional recurrent excitation (inverted Lincoln hat connectivity). Excitation is colour-coded (red is strong excitation; blue is strong inhibition).

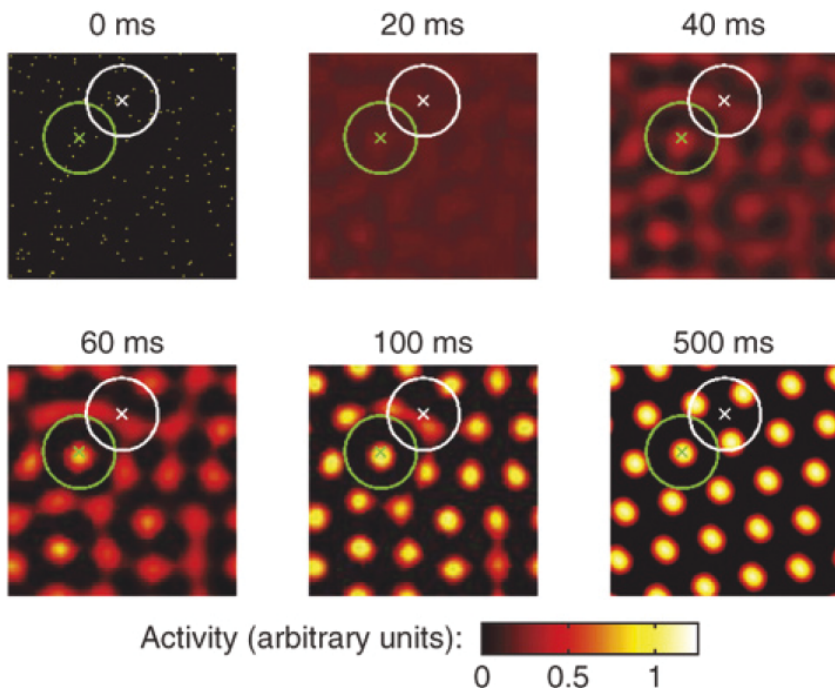


FIGURE 27. Hexagonal pattern formation on a two-dimensional lattice of stellate cells that have all-or-none inhibitory connectivity within a given radius. Neurons are arranged on the lattice according to their spatial phases. Connection radii for two example neurons are indicated by white and green circles. Activity is colour-coded, as indicated by the scale bar. Note low activity where circles overlap. Regions of low activity are regularly spaced. Note that hexagonal patterns are formed.

A problem with these models, in their original form, is that, at least among stellate cells in layer II of the medial entorhinal cortex, there is no recurrent excitation (Dhillon and Jones, 2000; Couey et al., 2013). However, in collaboration with Yasser Roudi and his colleagues, we have shown that hexagonally spaced patterns can be obtained exclusively by inhibitory surrounds, converting the Mexican hat of excitation and surrounding inhibition to an inverted Lincoln hat with only inhibition (Fig. 26b; Couey et al., 2013; Bonnevie et al., 2013). Once hexagonal firing is generated in a network with inverted Lincoln-hat all-or-none inhibitory connectivity, the network activity can be updated in accordance with the animal's position based on inputs that tell the network about the instantaneous speed of the animal (Fig. 25c) and, as a result, the grid pattern of the network will be reflected in the firing of individual neurons (Bonnevie et al., 2013).

Thus possible mechanisms of grid cell formation have been outlined. Data in support of these models are still scarce but new methods and technologies allow key predictions of the models to be tested. Testing the models, and developing them further, will certainly be among the main endeavours of scientists interested in grid cells during the years to come.

8. GENERAL PRINCIPLES OF NETWORK FUNCTION

Although a lot remains to be explored, I think we can say that the thousands of neuroscientists who have worked on cognitive maps have learnt much about the neural basis of space and maybe also cognition more generally. The entorhinal-hippocampal space system is one of the first cognitive functions to be understood in some mechanistic detail at the cell and cell-assembly level. In some sense the network of grid cells, border cells, head direction cells and place cells provides the components of the neural computations envisaged at the behaviour level by Tolman (1948) and at the cell assembly level by Hebb (1949). Moreover, what is particularly fascinating about grid cells is that they may inform us about general principles of neural pattern formation. Grid cells may for example offer a window to understanding continuous attractor mechanisms in the cortex, mechanisms that may be applied in different forms across the entire brain.

Studies of the space system may pave the way for quantitative analyses of neural ensemble coding, analyses that may draw on properties analysed in other physical systems that have been studied in more depth. Grid cells provide an example of this potential as hexagonal patterns are abundant in nature, appearing in widely different systems, as illustrated by chemical concentrations in reaction-diffusion systems (Turing, 1953; Edelstein-Keshet, 1988) and current vortices in superconductors (Abrikosov, 1957; Essman and Träuble, 1967). In many systems, the patterns are thought to arise as an equilibrium state following competitive interactions between the elements. In a superconductor, for example, current vortices may arrange themselves in a hexagonal pattern because of repulsive interactions between the vortices in the presence of an external magnetic field into the superconductor (Fig. 28; Essman and Träuble, 1967). It is our view that the principles underlying pattern formation in other physical and biological systems can shed light on pattern formation processes in the brain. The exploration of such common principles has barely started but I believe that, in the years to come, we will see many examples of neural computation where systems self-organise according to principles known to apply far beyond a particular brain system.

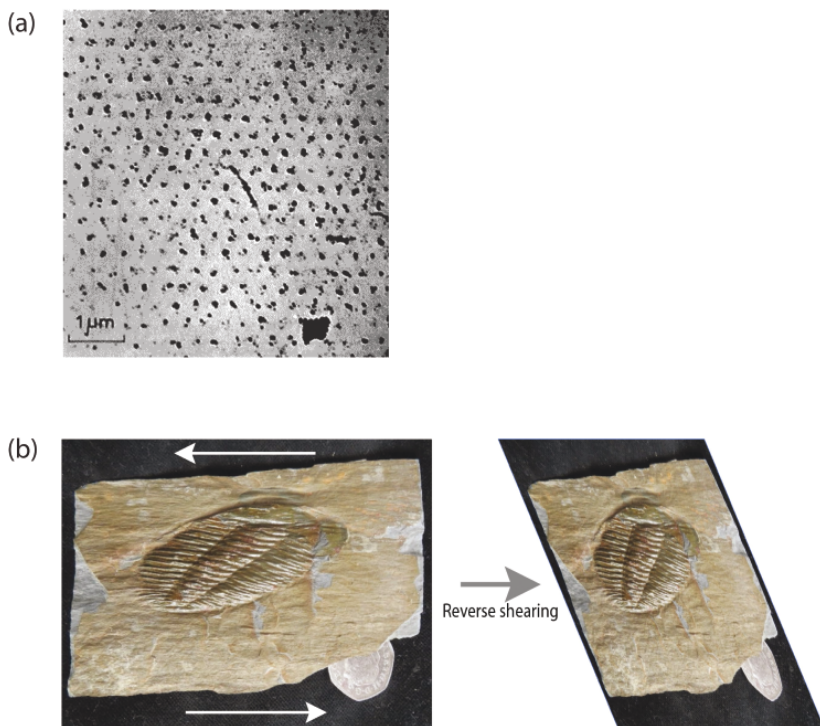


FIGURE 28. Neuroscience is beginning to understand some aspects of brain function in terms of underlying general principles of physics, as illustrated in (a) by the formation of Abrikosov current vortices through repulsive interactions in a superconductor exposed to an external magnetic field (Abrikosov, 1957; Essman and Träuble, 1967), and in (b) by inference of the original shape of a body, e.g. a trilobite, through reverse application of the shearing forces that once operated upon it. (a) is reproduced from Essman and Träuble (1967); (b) with permission from Pete Lawrence (www.bigfossil.com).

REFERENCES

1. Abrikosov AA (1957). Magnetic properties of superconductors of the second group. *Sov. Phys.-JETP (Engl. Transl.)*, **5**:6.
2. Andersen P (1971). Lamellar organization of hippocampal pathways. *Exp. Brain Res.* **13**, 222–238.
3. Barnes CA, McNaughton BL, Mizumori SJ, Leonard BW and Lin LH (1990). Comparison of spatial and temporal characteristics of neuronal activity in sequential stages of hippocampal processing. *Prog. Brain Res.* **83**, 287–300.
4. Bonnevie T *et al* (2013). Grid cells require excitatory drive from the hippocampus. *Nature Neurosci.* **16**, 309–317.

5. Bruce C, Desimone R and Gross CG (1981). Visual properties of neurons in a polysensory area in superior temporal sulcus in the macaque. *J. Neurophysiol.* **46**, 369–384.
6. Brun, VH, Otnass MK, Molden S, Steffenach HA, Witter MP, Moser M-B and Moser EI (2002). Place cells and place recognition maintained by direct entorhinal-hippocampal circuitry. *Science* **296**, 2243–2246.
7. Burak Y and Fiete IR (2009). Accurate path integration in continuous attractor network models of grid cells. *PLoS Comput. Biol.* **5**, e1000291.
8. Couey JJ *et al* (2013). Recurrent inhibitory circuitry as a mechanism for grid formation. *Nature Neurosci.* **16**, 318–324.
9. Dhillon A and Jones RS (2000). Laminar differences in recurrent excitatory transmission in the rat entorhinal cortex in vitro. *Neuroscience* **99**, 413–422.
10. Dolorfo CL and Amaral DG (1998). Entorhinal cortex of the rat: topographic organization of the cells of origin of the perforant path projection to the dentate gyrus. *J. Comp. Neurol.* **398**, 25–48.
11. Dombeck DA, Khabbaz AN, Collman F, Adelman TL and Tank DW (2007). Imaging large-scale neural activity with cellular resolution in awake, mobile mice. *Neuron* **56**, 43–57.
12. Dominisoru C, Kinkhabwala AA and Tank DW (2013). Membrane potential dynamics of grid cells. *Nature* **495**, 199–204.
13. Edelstein-Keshet L (1988). *Mathematical models in biology*. Vol. 46. New York: Birkhäuser-McGraw-Hill.
14. Essman U and Träuble H (1967). The direct observation of individual flux lines in type II superconductors. *Physics Letters* **24A**, 526–527.
15. Felleman DJ and van Essen DC (1991). Distributed hierarchical processing in the primate cerebral cortex. *Cereb. Cortex* **1**, 1–47.
16. Fenton AA *et al*. (2008). Unmasking the CA1 ensemble place code by exposures to small and large environments: more place cells and multiple, irregularly arranged, and expanded place fields in the larger space. *J. Neurosci.* **28**, 11250–11262.
17. Frank LM, Brown EN and Wilson M (2000). Trajectory encoding in the hippocampus and entorhinal cortex. *Neuron* **27**, 169–178.
18. Fuhs MC and Touretzky DS (2006). A spin glass model of path integration in rat medial entorhinal cortex. *J. Neurosci.* **26**, 4266–4276.
19. Fyhn M, Molden S, Witter MP, Moser EI and Moser M-B (2004). Spatial representation in the entorhinal cortex. *Science* **305**, 1258–1264.
20. Fyhn M, Hafting T, Treves A, Moser M-B and Moser EI (2007). Hippocampal remapping and grid realignment in entorhinal cortex. *Nature* **446**, 190–194.
21. Fyhn M, Hafting T, Witter MP, Moser EI and Moser M-B (2008). Grid cells in mice. *Hippocampus* **18**, 1230–1238.
22. Gray CM, Maldonado PE, Wilson M and McNaughton B (1995). Tetrodes markedly improve the reliability and yield of multiple single-unit isolation from multi-unit recordings in cat striate cortex. *J. Neurosci. Methods* **63**, 43–54.
23. Gross CG, Bender DB and Rocha-Miranda CE (1969). Visual receptive fields of neurons in inferotemporal cortex of the monkey. *Science* **166**, 1303–1306.

24. Gross CG, Rocha-Miranda CE and Bender DB (1972). Visual properties of neurons in inferotemporal cortex of the Macaque. *J. Neurophysiol.* **35**, 96–111.
25. Hafting T, Fyhn M, Molden S, Moser M-B and Moser EI (2005). Microstructure of a spatial map in the entorhinal cortex. *Nature* **436**, 801–806.
26. Hartley T, Burgess N, Lever C, Cacucci F and O’Keefe J (2000). Modeling place fields in terms of the cortical inputs to the hippocampus. *Hippocampus* **10**, 369–379.
27. Hebb DO (1949). *The Organization of Behavior*. New York: Wiley.
28. Heys JG, Rangarajan KV and Dombeck DA (2014). The functional micro-organization of grid cells revealed by cellular-resolution imaging. *Neuron* **84**, 1079–1090.
29. Hubel DH and Wiesel T (1959). Receptive fields of single neurones in the cat’s striate cortex. *J. Physiol. (Lond.)* **148**, 574–591.
30. Hubel DH and Wiesel T (1962). Receptive fields, binocular interaction, and functional architecture of cat striate cortex. *J. Physiol. (Lond.)* **160**, 106–154.
31. Hubel DH and Wiesel T (1977). Functional architecture of macaque monkey visual cortex. *Proc. R. Soc. B* **198**, 1–59.
32. Jacobs J *et al.* (2013). Direct recordings of grid-like neuronal activity in human spatial navigation. *Nature Neurosci.* **16**, 1188–1190.
33. Kandel ER (2000). Nobel Lecture: The Molecular Biology of Memory Storage: A Dialog between Genes and Synapses. *Nobelprize.org*. Nobel Media AB.
34. Kerr JND, Greenberg D and Helmchen F (2005). Imaging input and output of neocortical networks in vivo. *Proc. Natl. Acad. Sci. U. S. A.* **102**, 14063–14068.
35. Killian NJ, Jutras MJ and Buffalo EA (2012). A map of visual space in the primate entorhinal cortex. *Nature* **491**, 761–764.
36. Krubitzer L, Campi KL and Cooke DF (2011). All rodents are not the same: A modern synthesis of cortical organization. *Brain Behav. Evol.* **78**, 51–93.
37. Krupic J, Bauza M, Burton S, Lever C and O’Keefe J. How environment geometry affects grid cell symmetry and what we can learn from it. *Philos. Trans. R. Soc. Lond. B Biol. Sci.* **369**, 20130188 (2014).
38. Lashley KS (1929). *Brain Mechanisms and Intelligence: Quantitative Study of Injuries to the Brain*. Chicago: University of Chicago Press.
39. Lashley KS (1950). In search of the engram. *Society of Experimental Biology Symposium* **4**, 454–482.
40. Low RJ, Gu Y and Tank DW (2014). Cellular resolution optical access to brain regions in fissures: Imaging medial prefrontal cortex and grid cells in entorhinal cortex. *Proc. Natl. Acad. Sci. U.S.A.* **111**, 18739–18744.
41. Mase, G. *Continuum Mechanics*, p. 44–53 (McGraw-Hill Professional, 1970).
42. Mathis A, Herz AV & Stemmler M (2012). Optimal population codes for space: grid cells outperform place cells. *Neural Comput.* **24**, 2280–2317.
43. McNaughton BL *et al* (1996). Deciphering the hippocampal polyglot: The hippocampus as a path integration system. *J. Exp. Biol.* **199**, 173–185.
44. McNaughton BL, Battaglia FP, Jensen O, Moser EI and Moser M-B (2006). Path integration and the neural basis of the ‘cognitive map’. *Nature Rev. Neurosci.* **7**, 663–678.
45. Moser EI, Kropff E and Moser M-B (2008). Place cells, grid cells, and the brain’s spatial representation system. *Annu. Rev. Neurosci.* **31**, 69–89.

46. Moser EI et al. (2014). Grid cells and cortical representation. *Nature Rev. Neurosci.* **15**, 466–481.
47. Muller RU and Kubie JL (1987). The effects of changes in the environment on the spatial firing of hippocampal complex-spike cells. *J. Neurosci.* **7**, 1951–1968.
48. Ohki K, Chung S, Ch'ng YH, Kara P and Reid RC (2005). Functional imaging with cellular resolution reveals precise micro-architecture in visual cortex. *Nature* **433**, 597–603.
49. Ohki K, Chung S, Kara P, Hübener M, Bonhoeffer T and Reid C (2006). Highly ordered arrangement of single neurons in orientation pinwheels. *Nature* **442**, 925–928.
50. O'Keefe J (1976). Place units in the hippocampus of the freely moving rat. *Exp. Neurol.* **51**, 78–109.
51. O'Keefe J and Dostrovsky J (1971). The hippocampus as a spatial map. Preliminary evidence from unit activity in the freely-moving rat. *Brain Res.* **34**, 171–175 (1971).
52. O'Keefe J and Nadel L (1978). *The Hippocampus as a Cognitive Map* (Oxford: Clarendon Press).
53. Perrett DI, Rolls ET and Caan W (1982). Visual neurones responsive to faces in the monkey temporal cortex. *Exp. Brain Res.* **47**, 329–342.
54. Quirk GJ, Muller RU, Kubie JL and Ranck JB Jr (1992). The positional firing properties of medial entorhinal neurons: description and comparison with hippocampal place cells. *J. Neurosci.* **12**, 1945–1963.
55. Samsonovich A and McNaughton BL (1997). Path integration and cognitive mapping in a continuous attractor neural network model. *J. Neurosci.* **17**, 5900–5920.
56. Sargolini F, Fyhn M, Hafting T, McNaughton BL, Witter MP, Moser M-B and Moser EI (2006). Conjunctive representation of position, direction, and velocity in entorhinal cortex. *Science* **312**, 758–762.
57. Savelli F, Yoganarasimha D and Knierim JJ (2008). Influence of boundary removal on the spatial representations of the medial entorhinal cortex. *Hippocampus* **18**, 1270–1282.
58. Solstad T, Boccara CN, Kropff E, Moser M-B and Moser EI (2008). Representation of geometric borders in the entorhinal cortex. *Science* **322**, 1865–1868.
59. Stensola H, Stensola T, Solstad T, Frøland K, Moser M-B and Moser EI (2012). The entorhinal grid map is discretized. *Nature* **492**, 72–78.
60. Stensola T, Stensola H, Moser M-B and Moser EI (2015). Shearing-induced asymmetry in entorhinal grid cells. *Nature* **518**, 207–212.
61. Stettler DD and Axel R (2009). Representations of odor in the piriform cortex. *Neuron* **63**, 854–864.
62. Stosiek C, Garaschuk O, Holthoff K and Konnerth A (2003). In vivo two-photon calcium imaging of neuronal networks. *Proc. Natl. Acad. Sci. U.S.A.* **100**, 7319–7324.
63. Tanaka K, Saito H, Fukada Y and Moriya M (1991). Coding visual images of objects in the inferotemporal cortex of the macaque monkey. *J. Neurophysiol.* **66**, 170–189.
64. Tolman EC (1948). Cognitive maps in rats and men. *Psychol. Rev.* **55**, 189–208.
65. Tsao DY, Freiwald WA, Tootell RB and Livingstone MS (2005). A cortical region consisting entirely of face-selective cells. *Science* **311**, 670–674.

66. Tsodyks M and Sejnowski T (1995). Associative memory and hippocampal place cells. *Int. J. Neural Syst.* **6** (Suppl.), 81–86 (1995).
67. Turing A (1953). The chemical basis of morphogenesis, *Phil. Trans. Royal Soc. (part B)* **237**, 37–72.
68. Van Hooser SD, Heimel JA, Chung S, Nelson SB and Toth LJ (2005). Orientation selectivity without orientation maps in visual cortex of a highly visual mammal. *J. Neurosci.* **25**, 19–28.
69. Wei X-X, Prentice J and Balasubramanian V (2013). The sense of place: Grid cells in the brain and the transcendental number e. arXiv:1304.0031 [q-bio.NC].
70. Wilson MA and McNaughton BL (1993). Dynamics of the hippocampal ensemble code for space. *Science* **261**, 1055–1058.
71. Witter MP, Groenewegen HJ, Lopes da Silva FH and Lohman AHM (1989). Functional organization of the extrinsic and intrinsic circuitry of the parahippocampal region. *Prog. Neurobiol.* **33**, 161–254.
72. Yartsev MM, Witter MP and Ulanovsky N (2011). Grid cells without theta oscillations in the entorhinal cortex of bats. *Nature* **479**, 103–107.

Portrait photo of Edvard I. Moser by photographer Alexander Mahmoud.